Available online at www.sciencedirect.com
ScienceDirect
Journal of Power Sources 164 (2007) 678–687
JOURNAL OF POWER SOURCES
www.elsevier.com/locate/jpowsour

What is the design objective for portable power generation: Efficiency or energy density?

Alexander Mitsos [a], Benoît Chachuat [b], Paul I. Barton [a,*]

[a] *Department of Chemical Engineering, Massachusetts Institute of Technology, 66-464, 77 Massachusetts Avenue, Cambridge, MA 02139, United States*
[b] *Laboratoire d' Automatique, École Polytechnique Fédérale de Lausanne, Switzerland*

Received 29 August 2006; received in revised form 30 October 2006; accepted 31 October 2006
Available online 8 December 2006

Abstract

Recently, various alternatives to batteries, such as microfabricated fuel cell systems, have been proposed for portable power generation. In large-scale power production plants emphasis is placed on energy conversion efficiency. On the other hand, the intrinsic design objective for portable power generation devices is the energy density, i.e., the electrical energy generated from a given mass or volume of device and fuel cartridge. It is plausible to stipulate that an increase in the energy conversion efficiency of a system leads to an increase in energy density, but we demonstrate through theoretical analysis and case studies that the two metrics are not equivalent. In some cases, such as systems with a combination of fuels, maximizing efficiency leads to drastically different design, operation and performance than maximizing energy density. Another interesting observation is that, due to interaction between components, maximal component efficiency does not always imply maximal system efficiency.

Keywords: Micropower; Portable power generation; Fuel cell system; Micro fuel cell; Pareto optimal; Design metrics

1. Introduction

The increasing need for man-portable power generation for military and civilian applications is well established, e.g., [1,2]. The predominant technology is currently batteries, but there are technological, economical and ecological concerns. One of the problems is that the energy density, i.e., the energy produced per mass or volume of the battery, is relatively low, in the order of a few hundred $\mathrm{Wh\,l^{-1}}$ and $\mathrm{Wh\,kg^{-1}}$ for rechargeable batteries [3,4].

One of the promising alternative technologies is the use of microfabricated fuel cell-based systems with common fuels or chemicals, such as hydrocarbons or alcohols, as the energy source. The promise of this approach is that the energy density of these fuels is relatively high and fuel cells can, in principle, achieve high efficiencies [5,6]. Moreover, similarly to batteries, fuel cell systems have few or no moving parts, and run silently. In order to achieve portability the use of microfabricated devices, as opposed to conventional devices, is plausible [7].

The area of man-portable power generation is extremely active and there are several academic and commercial programs exploring microfabricated fuel cell systems. The vast majority of the literature deals with fabrication issues, which are outside the scope of this paper. There are a few contributions on scaling and system-level considerations [8–11], and some contributions on detailed modeling [12,13]. The reader is referred to the review articles by Holladay et al. [14] and by Maynard and Meyers [15], as well as the collection [16].

The focus of this paper is a thorough discussion of the appropriate design objective for portable power generation. We demonstrate that the design objective of maximal energy density is not necessarily equivalent to the objective of maximal energy efficiency, in the sense that the two objectives may lead to drastically different design and/or operation. We first analyze several cases for which the two objectives are not equivalent from a mathematical point of view and then we demonstrate through case studies that this difference indeed affects the optimal design and operation.

* Corresponding author. Tel.: +1 617 253 6526; fax: +1 617 258 5042.
E-mail addresses: amitsos@alum.mit.edu (A. Mitsos), bchachua@alum.mit.edu (B. Chachuat), pib@mit.edu (P.I. Barton).

0378-7753/$ – see front matter © 2006 Elsevier B.V. All rights reserved.
doi:10.1016/j.jpowsour.2006.10.088

Nomenclature

C_{Pi}	molar heat capacity of species i ($J\,mol^{-1}\,K^{-1}$)
e_{grav}	gravimetric energy density ($Wh\,kg^{-1}$)
e_{vol}	volumetric energy density ($Wh\,l^{-1}$)
F	Faraday constant ($C\,mol^{-1}$)
G_i°	molar gas phase Gibbs free energy of pure species i at reference pressure ($J\,mol^{-1}$)
H_i^g	molar enthalpy of species i, ideal gas ($J\,mol^{-1}$)
H_i^f	molar enthalpy of formation of species i ($J\,mol^{-1}$)
H_i^{heat}	heating value of species i ($J\,mol^{-1}$)
ΔH_i^{vap}	vaporization enthalpy of species i ($J\,mol^{-1}$)
$\Delta_r H$	enthalpy of reaction r ($J\,mol^{-1}$)
I	current (A)
$\mathfrak{I}$	set of species
$\mathfrak{J}$	set of elements
M	mass (kg)
MV_i	molar volume of species i ($l\,mol^{-1}$)
MW_i	molecular weight of species i ($kg\,mol^{-1}$)
$N_{i,j}$	molar flowrate of species i of stream j ($mol\,s^{-1}$)
P	pressure (bar)
P_{ref}	reference pressure (bar)
PW	power (W)
R	gas constant ($J\,mol^{-1}\,K^{-1}$)
T	temperature (K)
T_{amb}	ambient Temperature (298 K)
T_{ref}	reference Temperature (298 K)
U	voltage (V)
U_{loss}	overall heat transfer coefficient ($W\,m^{-2}\,K^{-1}$)
V	volume (m^3)
z	number of electrons exchanged

Greek letters

$\alpha_{i,j}$	number of atoms of element j in species i
ϵ	product of emissivity and view factor ($W\,m^2/W\,m^2$)
ε	tolerance
η	conversion efficiency
η_{SOFC}	SOFC efficiency (W/W)
ζ_r	conversion of reaction r ($mol\,s^{-1}/mol\,s^{-1}$)
μ_j	KKT multiplier corresponding to element j ($J\,mol^{-1}$)
ν_{ri}	stoichiometric coefficient of species i in reaction r
ξ_r	extent of reaction r ($mol\,s^{-1}$)
ρ_i	density of species i ($kg\,m^{-3}$)
σ_A	maximal allowable tensile stress (Pa)
τ	residence time (s)
$\tau_{mission}$	mission duration (time between refueling) (h)
Φ	air ratio ($mol\,s^{-1}/mol\,s^{-1}$)

2. Analysis of design objectives

In large-scale power production, emphasis is placed on efficient utilization of the fuel. This is because the fuel cost is of the same or higher order of magnitude as the fabrication cost of the power production system. In man-portable power production the economical and ecological operating costs are much smaller relative to the fabrication costs of the systems. Typically, different man-portable power generation systems are compared using the metric of energy density of the system [6]. The specific energy, or *gravimetric energy density* e_{grav}^{sys} [$Wh\,kg^{-1}$], is expressed as the electrical energy produced per unit mass of system [3] and the *(volumetric) energy density* e_{vol}^{sys} [$Wh\,l^{-1}$] is defined as the electrical energy produced per unit volume of the system

$$e_{grav}^{sys} = \frac{\tau_{mission} PW}{M^{sys}} \qquad e_{vol}^{sys} = \frac{\tau_{mission} PW}{V^{sys}},$$

where the mission duration $\tau_{mission}$ [h] is the time between refueling or recharging, PW [W] is the power output (assumed constant for simplicity), M^{sys} [kg] is the mass of the system, and V^{sys} [l] is the volume of the system. Depending on the application, either of the densities is more important. It is essential to define the system appropriately including the power generation devices as well as the fuel containers. The most promising application of fuel cell systems is for long mission durations [9,17]. For the limit of an infinite mission duration the system energy density approaches the *fuel energy density*, i.e., the power produced per unit massflow or volumetric flow of the fuel

$$e_{grav}^{fuel} = \frac{PW}{3600 \sum_i MW_i N_{i,in}} \qquad e_{vol}^{fuel} = \frac{PW}{3600 \sum_i MV_i N_{i,in}},$$

where $N_{i,in}$ [$mol\,s^{-1}$] is the inlet molar flowrate of species i, MW_i [$kg\,mol^{-1}$] is the molecular weight of species i, MV_i [$l\,mol^{-1}$] is the molar volume of species i at storage conditions, 3600 is the conversion factor from hours to seconds, and the summation is taken over all stored fuels.

Power generation is associated with heat generation, inversely proportional to the overall system efficiency, e.g., [18]; inefficient processes might be considered uncomfortable for portable applications because of the large heat generation, e.g., a cellular phone getting hot, or yield an undesired heat signature in the battlefield.

The overall energy conversion efficiency η^{sys} for a power system is given by the power generated divided by the chemical energy fed to the system per unit time, accounting for unreacted fuel

$$\eta^{sys} = \frac{PW}{\sum_i H_i^{heat} N_{i,in}}, \tag{1}$$

where H_i^{heat} [$J\,mol^{-1}$] is the heating value of species i, i.e., the heat released from complete combustion of one mole of species i at reference conditions $T_{ref} = 298$ K.

Often it is important to define the energy conversion efficiency of components of a system, e.g., the reforming reactor or the fuel cell, and sometimes alternative definitions of efficiency are plausible. For instance, the efficiency in the fuel cell can be defined as the quotient of power produced to chemical energy fed to the fuel cell per unit time or as the quotient of power produced to chemical energy consumed per unit time. One definition accounts for unreacted fuel while the other does not. The latter definition is more appropriate when the fuel cell effluents

are utilized in a burner. As is shown in the following for the case of one chemical reaction the fuel cell voltage is an appropriate metric for the energy conversion efficiency. The definition of the component efficiency gives

$$\eta_{\mathrm{FC}} = \frac{\mathrm{PW}}{\xi \Delta_r H(T_{\mathrm{amb}})},$$

where η_{FC} is the fuel cell efficiency, PW [W] is the power, ξ [mol s^{-1}] is the extent of the reaction, and $\Delta_r H(T_{\mathrm{amb}})$ [J mol^{-1}] is the corresponding enthalpy of reaction at ambient conditions. On the other hand, the power produced is given by the product of voltage U [V] and current I [A]

$$PW = UI.$$

The current is the product of the extent of reaction, the Faraday constant F [C mol^{-1}], and the number of electrons z exchanged in the oxidation of hydrogen (2 per molecule of H_2)

$$I = z\xi F,$$

and therefore

$$\eta_{\mathrm{SOFC}} = U \frac{Fz}{\Delta_r H(T_{\mathrm{amb}})}.$$

The system energy conversion efficiency is a function of the component efficiencies. For components in series the overall efficiency is the product of the individual efficiencies; for components in parallel the overall efficiency is the average of the component efficiencies weighted with the individual power levels. As is demonstrated in a following case study, improving an individual component efficiency does not necessarily imply that the energy conversion efficiency of the system will also be improved. This is due to the often complicated interaction between individual components.

The objective of maximal energy density is in general not equivalent to the objective of maximal efficiency. The simplest example illustrating this is a comparison between different fuels; choosing a fuel with high energy density can lead to a higher system energy density despite a lower efficiency. For instance a 35% efficient butane system has a higher energy density than a 70% efficient ammonia system (see Fig. 1 in [7]). A similar behavior is seen for systems with a combination of different fuels/chemicals, where energy density and energy conversion efficiency bear different weights on each species. Note that a combination of fuels leads to performance improvements in some cases [17]. The extreme case of species combination is the addition of water in steam reforming reactions, which does not (directly) affect the energy efficiency but greatly reduces the energy density, assuming that the water cannot be recycled but has to be carried along with the fuel. Another extreme example is the case that no ambient air is available for the oxidation reactions, e.g., for underwater or space applications, and an oxygen or air cartridge must be carried. The gases require significant storage volumes and cartridge mass, and the energy density is significantly lower compared to the use of ambient air [7]. On the other hand, the energy stored in the compressed gas is very small compared to the chemical energy of the fuels and therefore the metric of energy conversion efficiency does not account for the stored gas. Moreover, the use of pure oxygen may increase the energy conversion efficiency compared to the use of ambient air. For systems involving only one stored species i, the fuel energy density and efficiency are proportional, since

$$e_{\mathrm{grav}}^{\mathrm{fuel}} = \frac{\mathrm{PW}}{3600\mathrm{MW}_i N_{i,\mathrm{in}}}, \qquad e_{\mathrm{vol}}^{\mathrm{fuel}} = \frac{\mathrm{PW}}{3600 \sum_i \mathrm{MV}_i N_{i,\mathrm{in}}}$$

$$\eta^{\mathrm{sys}} = \frac{\mathrm{PW}}{H_i^{\mathrm{heat}} N_{i,\mathrm{in}}}$$

and therefore

$$\frac{e_{\mathrm{grav}}^{\mathrm{fuel}}}{\eta^{\mathrm{sys}}} = \frac{H_i^{\mathrm{heat}}}{3600\mathrm{MW}_i}, \qquad \frac{e_{\mathrm{vol}}^{\mathrm{fuel}}}{\eta^{\mathrm{sys}}} = \frac{H_i^{\mathrm{heat}}}{3600\mathrm{MV}_i}.$$

On the other hand, the system energy density is also a function of the device size, while the energy conversion efficiency is not.

3. Case studies

In this section we use different case studies to demonstrate that the design objectives of maximal energy density and maximal energy efficiency are not only different from a mathematical point of view, but may also lead to different optimal design and/or operation and therefore different performance. We first use the methodology for comparison of alternatives developed in [7,17], which is based on mass and energy balances along with prespecified parameters describing component performance. Then we use a kinetic-based case study based on the methodology for optimal design and operation of fixed process structures developed in [19]. Finally, we present an equilibrium-based case study. The three case studies are in a sense different extreme cases: the system-level case study allows the comparison of different fuels and different processes, but has some parameters that are not calculated from first principles; the results of the kinetic-based case study are limited by the effect of temperature on reaction rates and heat losses and are therefore scale-dependent; the results of the equilibrium-based case study are independent of chemical kinetics and heat losses. The reason for the variety of case studies is to demonstrate that the results are not an artifact of the methodology, but rather an intrinsic difference of the design objectives. Moreover, using different formulations we investigate the suitability of the design metrics for the selection of a process among alternatives (first case study) as well as for the optimal design operation of a given process (second and third case studies).

3.1. System-level case studies

In [7,17] a methodology for the comparison of micropower generation alternatives is presented. It is based on relatively simple models that are general enough to be independent of design details, such as the choice of catalysts and reactor configuration. Mass and energy balances are combined with user-specified parameters that describe the performance of the system components. Since heat integration and heat losses to the ambient are a crucial part of the design, they are considered in parallel with the flowsheeting options. This is done by combining units in conceptual stacks of uniform temperature and by calculating the

heat losses to the ambient based on the device surface area and constant conductive and radiative heat transfer coefficients. The energy balance is closed by oxidizing sufficient fuel in the burner units. Out of the thousands of possible process configurations and layouts in [17], here we compare four alternatives in terms of the achievable energy densities and energy efficiency. For the model details, including the calculation of fuel and system energy density the reader is referred to [7,17].

For all four alternatives we consider a power generation of $PW = 10\,\mathrm{W}$. For the calculation of system energy density a mission duration of $\tau_{\mathrm{mission}} = 30\,\mathrm{h}$ is assumed. Heat losses are accounted for with an overall transfer coefficient $U_{\mathrm{loss}} = 3\,\mathrm{W\,m^{-2}\,K^{-1}}$ and an emissivity (including the view factor) of $\epsilon = 0.2$. The operating pressure is assumed to be 1 atm for all four processes. Three out of the four processes employ atmospheric air. For these processes a pressure increase mechanism such as a microblower is assumed, with a power requirement of $3\,\mathrm{kJ\,mol^{-1}}$ of air fed to the system. This conservative power requirement is calculated assuming isothermal compression at ambient temperature from 1 to 1.2 atm with an efficiency of 15% [7]. The SOFC and burner operating temperatures are set to 1000 K and the outlet temperatures to 600 K. The conversion is assumed to be 90% in the reactor, 80% in the fuel cell and 95% in the burner. The residence time in the SOFC is assumed to be 20 ms and in the burner 1 ms. The effect of packaging and thermal insulation are accounted for by calculating the device volume as 10 times the inner volume of the reactors and fuel cell. A device density of $1\,\mathrm{kg\,l^{-1}}$ is assumed. The fuel cell power output is assumed to be 70% of the product of extent of reaction and standard Gibbs free energy of reaction calculated at the fuel cell temperature

$$\mathrm{PW} = 0.7 \sum_r \xi_r \sum_i \nu_{ri} G_i^{\circ}(T),$$

where ξ_r is the extent of electrochemical reaction r, ν_{ri} is the stoichiometric coefficient of species i in reaction r, and $G_i^{\circ}(T)$ is the molar gas phase Gibbs free energy of pure species i at the reference pressure. This simplification eliminates the dependence on composition.

The first alternative considered is the combination of ammonia cracking for the generation of hydrogen with a polymer electrolyte membrane (PEM) fuel cell (see Fig. 1). While ammonia is very toxic, it is considered as a hydrogen source, e.g., [20], because the cracking products do not contain carbon monoxide which is a poison for PEM fuel cells. To overcome heat losses and the endothermicity of ammonia decomposition, the fuel cell effluent from the anode compartment is oxidized. Note that using a new air stream for the hydrogen burner leads to a better performance than using the air excess from the fuel cell effluent of the cathode compartment, because of the low temperature of the PEM and the nitrogen and water that are present in it. The hydrogen burner and the cracking reactor are considered to be in an isothermal stack for better performance [17]. The residence time in the reactor is assumed to be 1 ms, the operating temperature 1000 K and the outlet temperature 600 K, accounting for partial heat recovery. Atmospheric air is used for the oxidation reactions with an energetic penalty as described above. The equilibrium concentration of ammonia at 1000 K is approximately 200 ppm and therefore a significant performance decrease of PEM may be observed [21,22]. Our models do not account for this degradation but for actual deployment this issue has to be addressed. A possibility is to use an ammonia sorbent, e.g., [23]. Including the weight and volume of this sorbent would affect the system energy density but not the conversion efficiency, thus strengthening our point that energy conversion efficiency is not the appropriate metric. We also neglect any need for cooling or humidifying of the PEM.

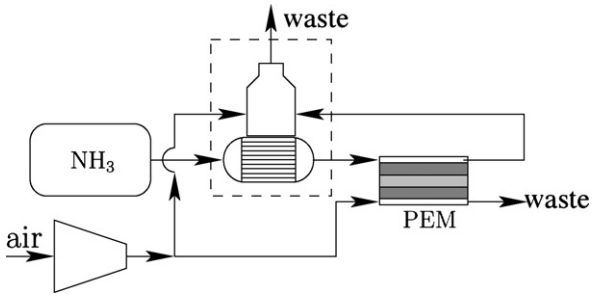

Fig. 1. Flowsheet for ammonia cracking.

The second alternative considered is methane oxidation in a direct solid-oxide fuel cell (SOFC) using compressed oxygen for the oxidation (see Fig. 2). At the macroscale steam reforming of natural gas is the predominant technology for hydrogen production. Methane as a feedstock for hydrogen production has the advantage that no carbon bonds need to be broken and the ratio of hydrogen-to-carbon atoms is maximal among the hydrocarbons. Moreover, compared with methanol and formic acid, methane has the advantage that it is not already partially oxidized. As a feedstock for portable applications it has the major drawback that it is supercritical at ambient temperatures and most likely to be stored as a compressed gas, which leads to low energy densities. The ideal case of direct electrochemical oxidation of methane in a SOFC is considered. As a further idealization we ignore the effect of carbon deposition on the catalysts. We assume gas storage in a plastic container with a maximal stress $\sigma_{\mathrm{max}} = 100\,\mathrm{MPa}$, a density of $\rho = 1.5\,\mathrm{kg\,m^{-3}}$ and a storage pressure of 10 MPa.

The third alternative considered is steam reforming of propane and oxidation of the generated hydrogen and carbon monoxide in a SOFC (see Fig. 3). Propane has the advantage that it has a high intrinsic energy density and can be stored as a liquid under moderate pressure. Moreover, the vapor pressure of propane is sufficient to overcome pressure losses and no compressor or pump is needed for the fuel. Atmospheric air is used for the oxidation reactions with an energetic penalty as described above. To overcome heat losses the fuel cell effluent is oxidized and since the SOFC operates at a high temperature the air excess

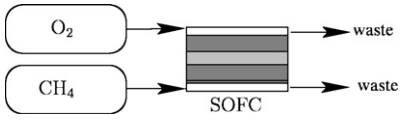

Fig. 2. Flowsheet for methane oxidation in a SOFC.

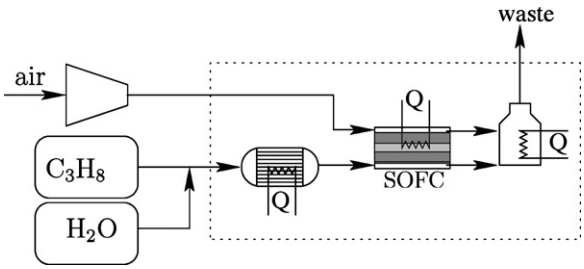

Fig. 3. Flowsheet for steam reforming of propane.

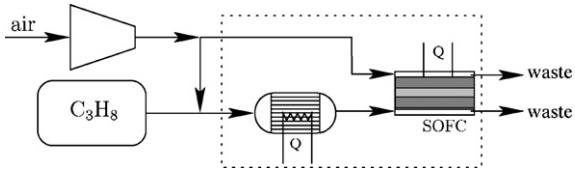

Fig. 4. Flowsheet for partial oxidation of propane.

from the fuel cell is used for the burner. The residence time in the reactor is assumed to be 2 ms, the operating temperature 1000 K and the outlet temperature 1000 K. A stoichiometric mixture of propane and water is used. The power generated in the SOFC is based on equivalent hydrogen production [17,24], i.e., it is assumed that CO and C_3H_8 undergo internal reforming and that only hydrogen is electrochemically oxidized.

The fourth alternative considered is partial oxidation of propane and oxidation of the generated hydrogen and carbon monoxide in a SOFC (see Fig. 4). Atmospheric air is used for the oxidation reactions with an energetic penalty as described above. The exothermicity of the partial oxidation reaction suffices to overcome the heat losses. The residence time in the reactor is assumed to be 1 ms, the operating temperature 1000 K and the outlet temperature 1000 K. The power generated in the SOFC is again based on equivalent hydrogen production [17,24].

The results of the comparison are summarized in Table 1. There are several interesting points to note. The partial oxidation of propane leads to the highest energy densities, despite the lowest energy conversion efficiency, while the direct oxidation of methane leads to the highest energy conversion efficiency but the lowest system energy densities. Both the system and fuel volumetric energy densities of methane direct oxidation are very low, due to the large volume required for the storage of the gases (methane and oxygen). Moreover, the gravimetric fuel energy density of methane is low, due to the mass of oxygen which is accounted for [17]. The large difference in gravimetric energy density of methane direct oxidation is due to the mass of the gas cartridges. Despite lower energy conversion efficiency, the propane-based processes lead to higher energy densities than the ammonia-based process, because of the intrinsic difference in energy density between the two fuels. The comparison of the two idealized possibilities of propane fuel processing reactions shows that the energy conversion efficiency is not a suitable metric for man-portable applications, because it does not account for the water weight and volume; the higher energy efficiency of steam reforming is due to the generation of additional hydrogen in the reactor. With the exception of the process requiring gas storage, the fuel energy density and system energy density give the same qualitative comparison among processes.

3.2. Kinetic-based study

In this case study we consider the ammonia-butane process from [19]. The power generation process consists of a fuel processing reactor, a solid-oxide fuel cell (SOFC) and two burners, fabricated in a single silicon stack fed with ammonia and butane fuels (Fig. 5). Ammonia is first catalytically decomposed into nitrogen and hydrogen. The produced gases are fed into the anode of the SOFC. An air stream is fed to the cathode of the SOFC. The anode and cathode effluents are finally mixed and fed into burner I, along with potentially a second air stream, for catalytic oxidation. In parallel, a mixture of butane (C_4H_{10}) and air is fed into burner II for catalytic oxidation to produce heat, thus maintaining the stack at a desired, sufficiently high temperature, despite the heat losses and the fact that ammonia decomposition is an endothermic reaction.

The energy efficiency is given by the power output divided by the product of heating value and molar flowrates (cf. Eq. (1)). Based on the heating values and molecular weights of butane and ammonia, maximizing energy conversion efficiency for a given power output is equivalent to minimizing $N_{NH_3} + 8.4N_{C_4H_{10}}$ whereas maximizing the energy density is equivalent to minimizing $N_{NH_3} + 3.4N_{C_4H_{10}}$. Indeed,

$$e^{\text{fuel}}_{\text{grav}} = \frac{\text{PW}}{3600 \sum_i \text{MW}_i N_{i,\text{in}}} = \frac{\text{PW}}{3600(0.017N_{NH_3} + 0.058N_{C_4H_{10}})}$$

and since PW is a constant

$$\max e^{\text{fuel}}_{\text{grav}} \Leftrightarrow \min(0.017N_{NH_3} + 0.058\, N_{C_4H_{10}}) \Leftrightarrow \min(N_{NH_3} + 3.4N_{C_4H_{10}}).$$

The heating values of butane and ammonia can be calculated to approximately 2.7×10^6 and 3.2×10^5 J mol^{-1}, respectively,

Table 1
Results for the comparison of processes

Performance metric	NH_3	CH_4	C_3H_8 ref.	C_3H_8 POX
Energy efficiency (%)	27	30	23	16
Volumetric fuel energy density (Wh l^{-1})	1570	170	1740	1920
Gravimetric fuel energy density (Wh kg^{-1})	2580	1610	2540	3900
Volumetric system energy density (Wh l^{-1})	1510	130	1650	1800
Gravimetric system energy density (Wh kg^{-1})	2370	320	2320	3340

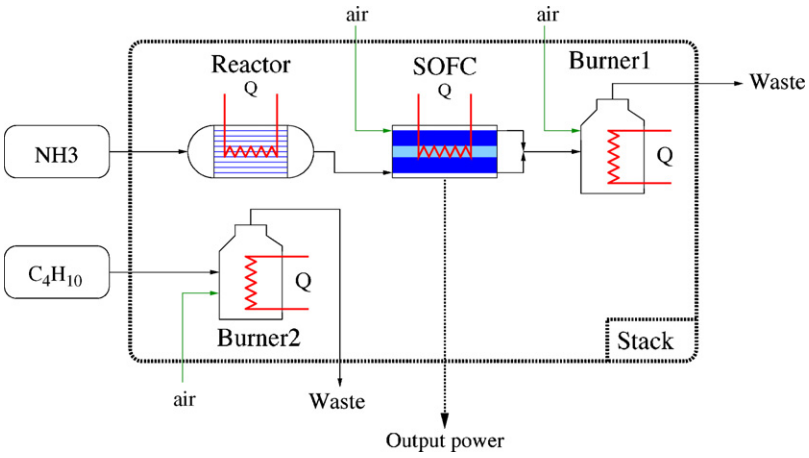

Fig. 5. Conceptual process flowsheet.

by the oxidation reactions and therefore

$$\eta^{\text{sys}} = \frac{\text{PW}}{\sum_i H_i^{\text{heat}} N_{i,\text{in}}} = \frac{\text{PW}}{3.2 \times 10^5 N_{\text{NH}_3} + 2.7 \times 10^6 N_{\text{C}_4\text{H}_{10}}}.$$

Since PW is a constant

$$\max \eta^{\text{sys}} \Leftrightarrow \min(3.2 \times 10^5 N_{\text{NH}_3} + 2.7 \times 10^6 N_{\text{C}_4\text{H}_{10}})$$
$$\Leftrightarrow \min(N_{\text{NH}_3} + 8.4 N_{\text{C}_4\text{H}_{10}}).$$

It is clear that the two objectives bear a different weight on each fuel flowrate and running the optimization problems shows that the respective optimal designs and operations are drastically different.

We use the same model as in [19], wherein the ammonia decomposition reactor, the solid-oxide fuel cell, and the fuel cell residual burner are modeled as isothermal and isobaric plug-flow reactors. The gas phase is assumed ideal, which is plausible because of the low pressure and high temperature. The change in density due to reaction is accounted for. For the kinetics of ammonia decomposition the reduced one-step expression from [25] is used. For the SOFC the kinetic data are taken by Achenbach [26]. For the oxidation of fuel cell effluents, the kinetic mechanism and data proposed by Pignet and Schmidt [27,28] are used. Nitrous oxide (N_2O) production is not accounted for and the unimolecular decomposition of NO is neglected. A lumped model, based on global mass and species balances, is formulated to describe butane catalytic combustion in burner II. It is assumed that the combustion reaction takes place to a fixed conversion and an excess of oxygen is always considered.

The optimal design and operation of the system is formulated as a nonlinear optimization problem with differential-algebraic equations embedded. The optimization variables are the sizes of the ammonia decomposition reactor, fuel cell and burner (design variables) as well as the fuel flowrates, air flowrates and fuel cell voltage. A common energy balance is considered for the device, accounting for heat losses to the ambient. Note that the fuel cell voltage affects both the power production and heat generation. We consider a power output of PW = 10 W with an operating temperature $T = 1000$ K, an outlet temperature $T_{\text{out}} = 650$ K and the same values for the various design parameters as in the base case of [19].

Table 2 summarizes the key findings for the two objective functions. When maximizing efficiency the achievable efficiency is approximately 25% higher compared to the case of maximizing energy density at the expense of a 10% reduction of the energy density. As expected from the weighting of the two fuel flowrates, maximizing the energy efficiency leads to a smaller butane flowrate at the expense of the ammonia flowrate.

A very interesting result is that the optimal device size is significantly smaller in the case of optimal efficiency, mostly due to a decrease in the fuel cell volume. Note that in the case of maximal energy density butane is not penalized as much and therefore the optimal design allows for a bigger device with a better hydrogen conversion in the fuel cell but higher heat losses, resulting in higher butane flowrates. On the other hand, in the case of maximal energy efficiency the optimal design is such that the ammonia line is nearly autothermal and a small butane flowrate is required to close the energy balance.

The fuel cell voltage in the case of maximal efficiency is significantly lower than in the case of maximal energy density. The most likely explanation is that in the case of optimal efficiency more heat generation is required from the fuel cell, which results in a lower efficiency and therefore lower voltage. This result also emphasizes the point that maximization of the efficiency of one component does not necessarily lead to maximization of the system efficiency.

Table 2
Performance parameters for kinetic-based case study

Property	Maximal energy density	Maximal energy efficiency
Energy density (Wh kg^{-1})	1247	1107
Energy efficiency (%)	17	21
Fuel cell conversion (%)	92	74
Fuel cell voltage (V)	0.43	0.33
Fuel cell efficiency (%)	44	33
Device inner volume (cm^3)	10.5	6.9
Ammonia flowrate ($\mu\text{mol s}^{-1}$)	89	145
Butane flowrate ($\mu\text{mol s}^{-1}$)	12	0.8

3.3. Equilibrium-based case study

In the last case study we consider equilibrium-limited production of hydrogen from octane via steam reforming and partial oxidation. We neglect heat losses, assuming that the power level is sufficiently high to justify this. This case study is therefore mostly relevant for applications in the order of 100s of Watts, where energy density is still an important consideration, but the scale is much larger than man-portable power generation where heat losses dominate [7]. Octane is used as a model fuel for gasoline. This approximation is adequate from the point of view of mass balance and chemical equilibrium but would not be appropriate for kinetic studies, and cannot capture catalyst poisoning effects. The above simplifications make the model independent of scale.

The design specification is to produce a fixed amount of hydrogen from octane, water and atmospheric air (see Fig. 6) with maximal fuel energy density or maximal efficiency. Assuming an ideal fuel cell operating at $T = 298$ K and $P = 1$ atm a metric for the energy of hydrogen is approximately 64 Wh $(\text{mol H}_2)^{-1}$ [7]. Note that we use this upper bound on fuel cell performance, to isolate the conversion efficiency of the fuel processing step from the fuel cell performance. The fuel energy density is therefore defined as the equivalent energy of hydrogen produced, divided by the massflow of octane and water:

$$e^{\text{fuel}}_{\text{grav}} = \frac{64 N_{\text{H}_2,\text{out}}}{\text{MW}_{\text{C}_8\text{H}_{18}} N_{\text{C}_8\text{H}_{18},\text{in}} + \text{MW}_{\text{H}_2\text{O}} N_{\text{H}_2\text{O},\text{in}}}.$$

Since the hydrogen production $N_{\text{H}_2,\text{out}}$ is fixed, maximizing the energy density is equivalent to minimizing the massflow of octane and water:

$$\max e^{\text{fuel}}_{\text{grav}} \Leftrightarrow \min(\text{MW}_{\text{C}_8\text{H}_{18}} N_{\text{C}_8\text{H}_{18}} + \text{MW}_{\text{H}_2\text{O}} N_{\text{H}_2\text{O}}).$$

The energy conversion efficiency is defined as the equivalent energy of the hydrogen produced, divided by the consumed heating value of octane approximately 1251 Wh $(\text{mol C}_8\text{H}_{18})^{-1}$:

$$\eta^{\text{reac}} = \frac{64 N_{\text{H}_2,\text{out}}}{1251 N_{\text{C}_8\text{H}_{18},\text{in}}}.$$

The energy conversion efficiency is proportional to the selectivity of hydrogen production, i.e., the molar flowrate of hydrogen produced divided by 9 times the molar flowrate of octane $(N_{\text{H}_2,\text{out}})/(9N_{\text{C}_8\text{H}_{18},\text{in}})$. Note that the selectivity can be greater than 1 from the conversion of water to hydrogen. Maximizing efficiency is equivalent to minimizing the molar flowrate of octane.

$$\max \eta^{\text{reac}} \Leftrightarrow \min(1251\, N_{\text{C}_8\text{H}_{18},\text{in}}) \Leftrightarrow \min(N_{\text{C}_8\text{H}_{18},\text{in}}).$$

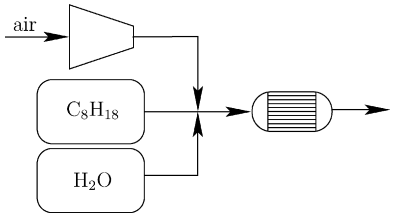

Fig. 6. Flowsheet for the equilibrium-based case study.

Note that for simplicity we do not account for the possibility of recycling, or further use of the excess water, carbon monoxide and methane.

We assume a single-stage reforming reactor operating in the temperature range $T = 800$–1200 K and at ambient pressure which allows all species to be treated as ideal gases. We assume that at the reactor outlet the gases are at chemical equilibrium. The embedded chemical equilibrium leads to a bilevel program [29]. The outer program corresponds to the optimal operation, i.e., the choice of inlet composition that maximizes the efficiency or energy density. Constraints in the outer program are the energy balance and the specified hydrogen production. The chemical equilibrium is embedded as the inner program. Due to convexity of the inner program, this bilevel program can be reformulated as a single level nonconvex optimization problem [30]. For the derivation of the model used (see Appendix A).

We solve the formulated optimization problem using BARON 7.5 [31] available through GAMS 22.2 [32]. The key results of maximizing the energy efficiency versus maximizing the energy density are shown in Table 3. The two objectives lead to drastically different operation as well as performance. Maximizing the energy conversion efficiency leads to a reduction of the energy density by approximately 60%. As expected, maximizing the energy conversion efficiency leads to a water rich feed, since the water molar flowrate does not affect the objective function. The maximal energy density is achieved at a significantly higher temperature (1125 K) than the maximal energy efficiency (899 K). In the case of maximal energy density, the idealized partial oxidation reaction

$$\text{C}_8\text{H}_{18} + 4\text{O}_2 \rightarrow 8\text{CO} + 9\text{H}_2$$

is a good approximation for the computed overall reaction

$$\text{C}_8\text{H}_{18} + 4.35\text{O}_2 \rightarrow 7.59\text{CO} + 8.56\text{H}_2 + 0.0334\text{CH}_4 + 0.366\text{CO}_2.$$

The computed overall reaction in the case of maximal energy conversion efficiency is not accurately described by one of the idealized reactions considered in [7] but rather from a combination of these reactions.

The above results were confirmed with Aspen Plus, version 12.1 [33], using an RGibbs reactor with the optimal inlet compositions and including the trace species that were neglected here. The discrepancy in the outlet composition is in the order of 1% while the discrepancy in the energy balance, due most likely to the constant heat capacity used, corresponds to an error in the temperature prediction of around 10 K.

To demonstrate the tradeoff between the two objective functions we also calculate the Pareto-optimal curve. A *Pareto-optimal* or *noninferior solution* is a set of decision variable values, such that if we try to improve one objective, the other will be degraded [29]. Maximizing the energy efficiency and energy density are the two extremes of the Pareto-optimal set (assuming unique optimal solutions [34]). The use of Pareto optimization is well established in multiobjective optimization, e.g., [29]. The Pareto curve can be obtained via the ε-constraint method, which in the case of two objectives is formulated as a

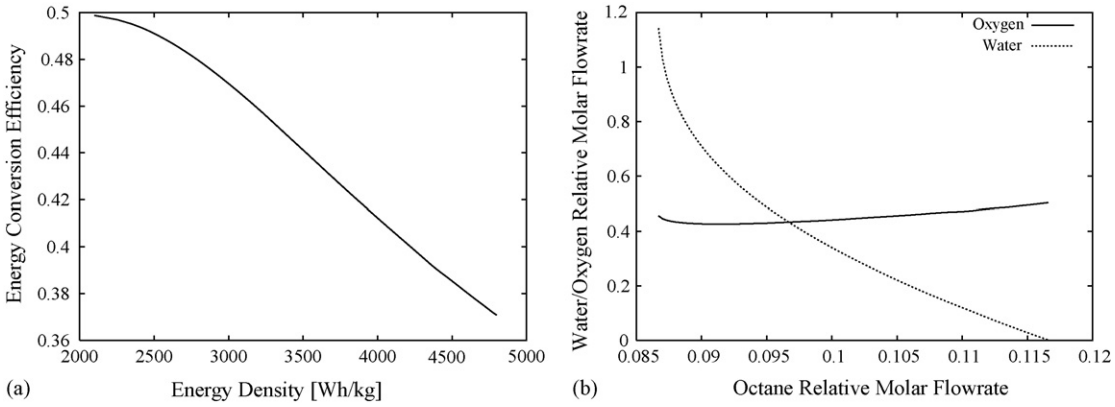

Fig. 7. Pareto optimal curve and inlet composition for the equilibrium-based octane reforming.

Table 3
Results for equilibrium-based case study

Property	Maximum energy density	Maximum energy efficiency
Octane relative molar flowrate $N_{C_8H_{18},in}/N_{H_2,out}$	0.117	0.087
Water relative molar flowrate $N_{H_2O,in}/N_{H_2,out}$	0.	1.18
Oxygen relative molar flowrate $N_{O_2,in}/N_{H_2,out}$	0.508	0.462
Temperature (K)	1125	899
Energy density (Wh kg^{-1})	4800	2050
Energy conversion efficiency (%)	37	50
Hydrogen selectivity (%)	96	130

single-parameter right-hand-side parametric optimization program [29]. We approximate this program by discretization with 50 equidistant points in the energy efficiency space. The results are shown in Fig. 7. On the left side we show the Pareto curve, i.e., the maximal energy density as a function of the energy efficiency, and on the right side the corresponding relative molar flowrates of oxygen and water as a function of the relative molar flowrate of octane. The high consumption of octane corresponds to a high energy density and a low energy efficiency.

The tradeoff between the two objectives is nearly linear. The increase of octane flowrate is associated with a slight increase in oxygen and a very pronounced decrease in water flowrate.

4. Conclusions and future work

For portable, and especially man-portable applications, the appropriate performance metric and design objective is energy density [6]. On the other hand, in large-scale power generation and energy conversion, the dominant objective is maximizing the energy conversion efficiency. We showed through analysis and case studies that these two objectives may lead to very different design, operation and/or performance. In particular we showed that energy efficiency is not a suitable metric for selecting, designing nor operating portable power generation devices, i.e., neither for choosing a given process among a list of candidate alternatives nor for finding the optimal design and operation parameters of a given alternative.

The models used largely neglect peripheral components such as valves and pumps, under the assumption that the influence of these components is not significant. Accounting for these components is of interest. We focused on fuel cell systems, but most observations are directly applicable to other systems transforming chemical to electrical energy, such as the use of thermophotovoltaic cells [35–37] or a microturbine driving a generator [38]. Also, studying hybrid electrochemical systems with a combination of a battery/super capacitor and a fuel cell is of interest.

Acknowledgments

This work was supported by the DoD Multidisciplinary University Research Initiative (MURI) program administered by the Army Research Office under Grant DAAD19-01-1-0566.

We would like to thank the anonymous reviewers for their useful suggestions that considerably improved the final form of this paper.

Appendix A. Equilibrium-based model

The chemical equilibrium of a set of species $i \in \mathfrak{I}$ containing elements $j \in \mathfrak{J}$ is formulated as a nonlinear minimization problem with linear constraints and a strictly convex objective function [39]

$$\min_{\mathbf{N}_{out}} \sum_{i\in\mathfrak{I}} N_{i,out}\left(G_i^{\circ}(T) + RT\,\ln\left(\frac{P}{P_{ref}}\right) + RT\,\ln\left(\frac{N_{i,out}}{\sum_{k\in\mathfrak{I}} N_{k,out}}\right)\right)$$

$$\text{s.t.} \sum_{i\in\mathfrak{I}} \alpha_{i,j} N_{i,out} = \sum_{i\in\mathfrak{I}} \alpha_{i,j} N_{i,in}, \quad \forall j \in \mathfrak{J}$$

$$N_{i,out} \geq 0, \quad \forall i \in \mathfrak{I},$$

where $N_{i,in}$ and $N_{i,out}$ for $i \in \mathfrak{I}$ denote the molar flow of species i into and out of the reactor, respectively. Note that the convexity of the objective function is with respect to the optimization variables (molar flowrates) and not with respect to parameters (temperature, pressure). The coefficients $\alpha_{i,j}$ correspond to the number of atoms of element j in species i. $G_i^{\circ}(T)$ denotes the molar Gibbs free energy of the pure species i at the reference pressure P_{ref} in the gas phase. Because of the logarithmic term, for implementation a nonzero lower bound needs to be imposed

on the molar flowrates $N_{i,\text{out}} \geq \varepsilon > 0$ and this causes problems with trace species. We consider operation at ambient pressure, and take this as the reference pressure.

To alleviate numerical difficulties, and based on the operating conditions and previous calculations of chemical equilibria [7], we make some further simplifying assumptions. Nitrogen N_2 is treated as an inert, neglecting the formation of nitrogen oxides and ammonia. This simplification is justified since the formation of nitrogen compounds is negligible from an mass and energy balance perspective and useful since it eliminates several species and an atom balance. Furthermore, complete conversion of oxygen and octane is assumed. This assumption is justified since, for the range of inlet compositions and temperatures considered, these species are only found in trace amounts at equilibrium. It is useful since the elimination of trace species makes the numerical behavior much more benign. Finally, we consider that the only hydrocarbon formed is methane. This simplification is again based on previous calculations [7], and is useful since it reduces the number of species. Since some species are eliminated, we distinguish between the set of inlet species $\mathfrak{I}_{\text{in}} = \{C_8H_{18}, H_2O, O_2\}$ and the set of outlet species $\mathfrak{I}_{\text{out}} = \{H_2O, H_2, CO, CO_2, CH_4\}$. Note that nitrogen is eliminated $N_{N_2,\text{out}} = N_{N_2,\text{in}} = 3.79 N_{O_2,\text{in}}$. The set of elements is given by $\mathfrak{J} = \{C, H, O\}$.

It can be easily verified that all molar flowrates $N_{i,\text{out}}$ are at nonzero value and therefore the inner program is equivalent to the following stationarity conditions (in addition to the element balances)

$$G_i^\circ(T) + RT \ln \frac{N_{i,\text{out}}}{N_{N_2,\text{out}} + \sum_{k\in\mathfrak{I}_{\text{out}}} N_{k,\text{out}}} + \sum_{j\in\mathfrak{J}} \alpha_{i,j}\mu_j = 0, \quad \forall i \in \mathfrak{I}_{\text{out}},$$

where μ_j is the KKT multiplier associated with the balance of atom j. This formulation avoids the complementarity slackness conditions that are usually encountered when a bilevel program is transformed to a single-level program.

Assuming a constant heat capacity C_P and since the outlet is gaseous,

$$G_i^\circ(T) = H_i^{\text{g}}(T_{\text{ref}}) + C_{Pi}(T - T_{\text{ref}}) - T\left(\frac{H_i^{\text{g}}(T_{\text{ref}}) - G_i^\circ(T_{\text{ref}})}{T_{\text{ref}}} + C_{Pi}\ln\left(\frac{T}{T_{\text{ref}}}\right)\right),$$

where $H_i^{\text{g}}(T_{\text{ref}})$ is the ideal gas enthalpy of species i at reference temperature.

Neglecting any heat losses, assuming that the outlet gases are at the reactor temperature, and that the inlet is at reference conditions (reference temperature $T_{\text{ref}} = T_{\text{amb}} = 298\,\text{K}$) the energy balance is given by

$$\sum_{i\in\mathfrak{I}_{\text{out}}} N_{i,\text{out}}\left(H_i^{\text{g}}(T_{\text{ref}}) + C_{Pi}(T - T_{\text{ref}})\right) = \sum_{i\in\mathfrak{I}_{\text{in}}} N_{i,\text{in}} H_i^{\text{f}}(T_{\text{ref}}).$$

At reference conditions, water and octane are liquids at ambient conditions, while all other species are gases. Therefore $H_i^{\text{f}}(T_{\text{ref}}) = H_i^{\text{g}}(T_{\text{ref}})$ for $i \notin \{H_2O, C_8H_{18}\}$ and $H_i^{\text{f}}(T_{\text{ref}}) = H_i^{\text{g}}(T_{\text{ref}}) - \Delta H_i^{\text{vap}}(T_{\text{ref}})$ for $i \in \{H_2O, C_8H_{18}\}$, where $\Delta H_i^{\text{vap}}(T_{\text{ref}})$ is the vaporization enthalpy at the reference temperature. The enthalpies and Gibbs free energies in the gas phase and T_{ref} are taken from [40], while the heat capacities and enthalpies of vaporization from [41], and are given in Table A.1.

The optimal operation problem is formulated as the following single-level nonlinear program

$$\begin{aligned}
&\min_{\mathbf{N}_{\text{out}},\mathbf{N}_{\text{in}},T,\boldsymbol{\mu}} f(\mathbf{N}_{\text{in}})\\
&\text{s.t. } 3.79 N_{O_2,\text{in}}(C_{PN_2}(T - T_{\text{ref}})) + \sum_{i\in\mathfrak{I}_{\text{out}}} N_{i,\text{out}}(H_i^{\text{g}}(T_{\text{ref}}) + C_{Pi}(T - T_{\text{ref}})) - \sum_{i\in\mathfrak{I}_{\text{in}}} N_{i,\text{in}} H_i^{\text{f}}(T_{\text{ref}}) = 0\\
&\sum_{i\in\mathfrak{I}_{\text{out}}} \alpha_{i,j} N_{i,\text{out}} - \sum_{i\in\mathfrak{I}_{\text{in}}} \alpha_{i,j} N_{i,\text{in}} = 0, \quad \forall j \in \mathfrak{J}\\
&H_i^{\text{g}}(T_{\text{ref}}) + C_{Pi}(T - T_{\text{ref}}) - T\left(\frac{H_i^{\text{g}}(T_{\text{ref}}) - G_i^\circ(T_{\text{ref}})}{T_{\text{ref}}} + C_{Pi}\ln\left(\frac{T}{T_{\text{ref}}}\right)\right)\\
&\quad + RT\ln\frac{N_{i,\text{out}}}{3.79 N_{O_2,\text{in}} + \sum_{k\in\mathfrak{I}_{\text{out}}} N_{k,\text{out}}} + \sum_{j\in\mathfrak{J}} \alpha_{i,j}\mu_j = 0, \quad \forall i \in \mathfrak{I}_{\text{out}}\\
&N_{H_2,\text{out}} = 1\\
&N_{i,\text{out}} \geq 0, \quad \forall i \in \mathfrak{I}_{\text{out}}\\
&N_{i,\text{in}} \geq 0, \quad \forall i \in \mathfrak{I}_{\text{in}}\\
&\mu_j \in \mathbb{R}, \quad \forall j \in \mathfrak{J},
\end{aligned}$$

where $f(\mathbf{N}_{\text{in}})$ is one of the two equivalent objective functions, i.e.,

$$f(\mathbf{N}_{\text{in}}) = N_{C_8H_{18},\text{in}}$$

for the energy conversion efficiency, or

$$f(\mathbf{N}_{\text{in}}) = \text{MW}_{C_8H_{18}} N_{C_8H_{18},\text{in}} + \text{MW}_{H_2O} N_{H_2O,\text{in}}$$

for the energy density.

The formulated nonlinear program (NLP) contains nonconvex functions and therefore global optimization methods are

Table A.1
Physical properties

Species	$H_i^g(T_{ref})$ [J mol^{-1}]	$\Delta H^{vap}(T_{ref})$ [J mol^{-1}]	$G_i{}^\circ(T_{ref})$ [J mol^{-1}]	C_{Pi}^g [J mol^{-1} K^{-1}]
N_2	0	N/A	0	30
O_2	0	N/A	0	32
H_2	0	N/A	0	29
H_2O	-242×10^3	40×10^3	-229×10^3	36
CO	-110×10^3	N/A	-137×10^3	30
CO_2	-394×10^3	N/A	-395×10^3	47
CH_4	-75×10^3	N/A	-51×10^3	50
C_8H_{18}	-208×10^3	42×10^3	-140×10^3	150

employed for its solution. It is relatively small with eleven variables and two degrees of freedom and therefore can be solved easily to guaranteed global optimality with general purpose solvers. The degrees of freedom are two of the three inlet molar flowrates $N_{C_8H_{18},in}$, $N_{H_2O,in}$ and $N_{O_2,in}$. The operating temperature is fixed by the energy balance. By the assumed constant heat capacity, the temperature could be eliminated from the set of variables by explicitly solving the energy balance, but this elimination is likely to make the optimization problem more difficult to solve.

References

[1] R. Jacobs, H. Christopher, R. Hamlen, R. Rizzo, R. Paur, S. Gilman, IEEE Aerospace Electron. Syst. Mag. 11 (6) (1996) 19–23.
[2] N. R. C. C. of Soldier Power/Energy Systems, Meeting the Energy Needs of Future Warriors, National Academies Press, 2004.
[3] D. Linden, Handbook of Batteries, McGraw-Hill, 2001.
[4] R.J. Brodd, Electrochem. Soc. Interface 8 (3) (1999) 20–23.
[5] C.K. Dyer, Nature 343 (6258) (1990) 547–548.
[6] C.K. Dyer, Sci. Am. 281 (1) (1999) 88–93.
[7] A. Mitsos, I. Palou-Rivera, P.I. Barton, Ind. Eng. Chem. Res. 43 (1) (2004) 74–84.
[8] D. Browning, P. Jones, K. Packer, J. Power Sources 65 (1–2) (1997) 187–195.
[9] C.K. Dyer, J. Power Sources 106 (1–2) (2002) 31–34.
[10] S. Atkinson, Membr. Technol. 2002 (1) (2002) 10–12.
[11] S.-W. Cha, R.O. Hayre, F.B. Prinz, Solid State Ionics 175 (1–4) (2004) 789–795.
[12] C. Hebbling, A. Heinzel, D. Golombowski, T. Meyer, M. Müller, M. Zedda, IMRET 3, Frankfurt, Germany, 1999, pp. 383–401.
[13] C. Cao, Y. Wang, J.D. Holladay, E.O. Jones, D.R. Palo, AIChE J. 51 (3) (2005) 982–988.
[14] J.D. Holladay, Y. Wang, E. Jones, Chem. Rev. 104 (10) (2004) 4767–4789.
[15] H.L. Maynard, J.P. Meyers, J. Vacuum Sci. Technol. 20 (4) (2002) 1287–1297.
[16] A. Mitsos, P.I. Barton, Publications on Portable Power Generation, http://yoric.mit.edu/download/reports/micropowerpub.pdf, Tech. Rep., Massachusetts Institute of Technology, 2006.
[17] A. Mitsos, M.M. Hencke, P.I. Barton, AIChE J. 51 (8) (2005) 2199–2219.
[18] J.P. Meyers, H.L. Maynard, J. Power Sources 109 (1) (2002) 76–88.
[19] B. Chachuat, A. Mitsos, P.I. Barton, Chem. Eng. Sci. 60 (16) (2005) 4535–4556.
[20] R. Metkemeijer, P. Achard, J. Power Sources 49 (1–3) (1994) 271–282.
[21] H.J. Soto, W.K. Lee, J.W.V. Zee, M. Murthy, Electrochem. Solid State Lett. 6 (7) (2003) 133–A135.
[22] R. Halseid, P.J.S. Vie, R. Tunold, J. Power Sources 154 (2) (2006) 343–350.
[23] N. Sifer, K. Gardner, J. Power Sources 132 (1–2) (2004) 135–138.
[24] Fuel Cell Handbook, fifth ed., EG&G Services; Parsons, Inc., Science Applications International Corporation, 2000.
[25] S.R. Deshmukh, A.B. Mhadeshwar, D.G. Vlachos, Ind. Eng. Chem. Res. 43 (12) (2004) 2986–2999.
[26] E. Achenbach, J. Power Sources 49 (1–3) (1994) 333–348.
[27] T. Pignet, L.D. Schmidt, Chem. Eng. Sci. 29 (5) (1974) 1123–1131.
[28] T. Pignet, L.D. Schmidt, J. Catal. 40 (2) (1975) 212–225.
[29] P.A. Clark, A.W. Westerberg, Comput. Chem. Eng. 7 (4) (1983) 259–278.
[30] J.F. Bard, Practical Bilevel Optimization: Algorithms and Applications, Nonconvex Optimization and Its Applications, Kluwer Academic Publishers, Dordrecht, 1998.
[31] N.V. Sahinidis, J. Global Optimization 8 (1996) 201–205.
[32] A. Brooke, D. Kendrick, A. Meeraus, GAMS: A User's Guide, The Scientific Press, Redwood City, CA, 1988.
[33] ASPENPLUS User's Guide, Aspen Tech, Cambridge, MA, 1988.
[34] B.S. Ahmad, P.I. Barton, Comput. Chem. Eng. 23 (10) (1999) 1365–1380.
[35] T.J. Coutts, Renewable Sustainable Energy Rev. 3 (2) (1999) 77–184.
[36] W.M. Yang, S.K. Chouand, C. Shu, Z.W. Li, H. Xue, Appl. Thermal Eng. 22 (16) (2002) 1777–1787.
[37] O.M. Nielsen, L.R. Arana, C.D. Baertsch, K.F. Jensen, M.A. Schmidt, Transducers 03 The 12th International Conference on Solid State Sensors, Actuators and Microsystems, 2003, pp. 714–717.
[38] A.H. Epstein, S.D. Senturia, Science 276 (5316) (1997) 1211.
[39] W.R. Smith, R.W. Missen, Chemical Reaction Equilibrium Analysis: Theory and Algorithms, John Wiley & Sons, New York, 1982.
[40] R.C. Reid, J.M. Prasunitz, B.E. Poling, The Properties of Gases and Liquids, McGraw Hill, New York, 1987.
[41] P.J. Linstrom, W.G. Mallard (Eds.), NIST Chemistry WebBook, National Institute of Standards and Technology, Gaithersburg, MD, 20899, 2003, http://webbook.nist.gov (NIST Standard Reference Database Number 69, March 2003).